Pollution 2022, 8(3): 1076-1087
DOI: 10.22059/POLL.2022.339417.1377

RESEARCH PAPER

Evaluation of Slow-Pyrolysis Process Effect on Adsorption Characteristics of Cow Bone for Ni Ion Removal from Ni-Contaminated Aqueous Solutions

Mahboub Saffari[1*], Masomeh Moazallahi[2]

[1] Department of Environment, Institute of Science and High Technology and Environmental Sciences, Graduate University of Advanced Technology, Kerman, Iran
[2] Institute of Science and High Technology and Environmental Sciences, Graduate University of Advanced Technology, Kerman, Iran

Received: 19.02.2022, Revised: 28.04.2022, Accepted: 01.05.2022

Abstract
The optimization of nickel ion (Ni^{2+}) removal in aqueous solutions with various factors (initial Ni concentration, solution pH, adsorbent dosage, contact time), as affected by raw cow bone (RBO) and its biochar (bone char: BC; produced by pyrolysis processes at 500 °C and a residence time of 4 hours) as adsorbents was investigated by a three-level Box–Behnken model (BBM) under response surface methodology (RSM). A total of 29 experimental runs were set for each adsorbent, and the experimental data were fitted to the empirical model. To understand the Ni^{2+} adsorption processes better, the properties of RBO and BC were characterized using Fe-SEM, FT-IR, BET, XRD, and CHNS elemental analysis techniques. The BC characteristics showed that pyrolysis increased the specific surface area (by 100 times) and phosphate functional groups, but decreased the carbonate functional groups, and yielded a more irregular and rougher morphological surface compared to RBO. Based on BC's superior ion exchange mechanisms and physical electrostatic adsorption compared to RBO, the removal efficiency of Ni^{2+} by BC was higher in aqueous solutions. The numerical optimization of BBM revealed that the optimum removal by BC (82.56%) was obtained at an initial Ni^{2+} concentration of 30.79 mg L^{-1}, pH of 6.99, adsorbent dose of 4.87 g L^{-1}, and contact time of 57.82 min, with the desirability of "1". BC can be effectively used for Ni removal from Ni-contaminated aqueous solutions; still, the application of modification methods (e.g., physical and chemical activation) may be necessary to help remove more Ni^{2+} by BC.

Keywords: Aqueous solutions; Bone char; Heavy metals; Response surface methodology; Sorption

INTRODUCTION

Nickel, as a toxic heavy metal, is widely used in manufacturing industries such as stainless steel, Ni alloys, and rechargeable batteries (Genchi et al., 2020). This element is usually present in the environment as a divalent ion, and its concentration in the environment causes various cancers (e.g., lung, nose, and bone cancers) in humans (Genchi et al., 2020). More than 40% of the Ni in the environment is produced by industrial plants, which has a significant share in surface water pollution. The Ni concentration in industrial wastewater is in the range of 3 to 100 mg l^{-1} and the maximum allowable Ni concentration in drinking water is 7 µg l^{-1} (Ida et al., 2021).

Water pollution with heavy metals such as Ni is a major environmental challenge that has

* Corresponding author Email: mahboobsaffari@gmail.com

seriously endangered the health of human societies. In recent decades, various methods have been adopted to purify water contaminated with these elements. At low contamination, the adsorption method is one of the most effective and cost-effective methods of water purification in which an inexpensive and environmentally friendly adsorbent with high adsorption capacity is selected. Nowadays, due to the high price of some adsorbents (nanoparticles, activated carbon, polymers) for heavy metal removal, the use of inexpensive compounds such as agricultural and livestock compounds is expanding (Saffari et al., 2018). However, the low efficiency of some natural adsorbents in heavy metal removal has motivated the application of various activation strategies to promote the adsorbents' adsorption properties (Saffari et al., 2018). One method for natural adsorbent activation is the pyrolysis process in which natural biomass is pyrolyzed at high temperatures under anaerobic conditions, thereby altering the specific surface area and functional groups (Saffari et al., 2018).

Bone is a waste of the meat industry with an annual production of >500,000 tons and containing important compounds such as hydroxyapatite as a special adsorbent of various pollutants. The process of pyrolysis, or partial calcination of bone, produces a compound known as bone char with unique properties compared to raw bone, which is used in the treatment of organic and inorganic contaminants in wastewater and industrial effluents (Hassan et al., 2008). It is utilized as a versatile adsorbent to remove a wide range of contaminants, including heavy elements, fluoride, and dyes (Wang et al., 2020; Ghanizadeh & Asgari, 2011; Alkurdi et al., 2019, 2020; Shahid et al., 2019, 2020). According to the literature, bone chars cause the adsorption of pollutants in aqueous solutions with three mechanisms of ion exchange, dissolution and precipitation reactions, and complex formation with pollutants (Mendoza–Castillo et al., 2015). In addition to the high heavy metal sorption potential on its surface structure, the presence of hydroxyapatite in the main structure of bone char leads to the exchange of Ca with elemental ions, thereby removing this element from aqueous solutions (Pan et al., 2009).

Adsorption of elements in aqueous solutions by the adsorbent is affected by various factors, e.g., contaminant concentration, adsorbent dose, contact time, solution pH, and solution temperature (Saffari et al., 2018). Evaluating the effects of each factor individually and their interactions on the removal percentage with conventional statistical methods not only complicates the interpretations, but also wastes a lot of time and money. To overcome this problem, the response surface methodology (RSM) is adopted for optimization studies. The RSM is a set of statistical techniques and applied mathematics for constructing experimental models. It aims to optimize the response (output variable), which is affected by several independent variables (input variables). Therefore, RSM can better predict and interpret the effects of various factors on contaminants removal by each adsorbent (Saffari et al., 2018). Despite a few studies on the removal of heavy metals by BC, no comparison of the adsorption properties and effects has so far been performed between RBO and the resulting biochar on Ni removal in aquatic environments. Thus, herein, after identifying and evaluating the properties of raw bone and its biochar, the Ni removal from the aqueous solution, as affected by various factors, was evaluated using RSM.

MATERIALS AND METHODS

Raw cow leg bones were first dried at dry room temperature and washed with hot water in triplicate for 10 minutes to remove fats, proteins, and impurities from the bone surface. Next, the washed bones were dried at 110 °C for 24 hours, crushed into small particles (0.5-1 cm), and transported into a biochar reactor. The studied bone char was made at 500 °C and a residence time of 4 hours in the presence of nitrogen gas (5 L min^{-1} for 5 min). The raw bone and bone char were crushed into small particles (10-20 μm) and kept in a desiccator for the Ni removal test. The physical, chemical, and morphological characteristics of the studied adsorbents were

determined using X-ray diffraction analysis (Bruker D8 Advance X-ray diffractometer: XRD), Fe-SEM (TESCAN FE-SEM MIRA3), FT-IR (TENSOR II from Bruker), BET (BELSORP Mini II), and CHNS elemental analysis (vario MACRO CHNS) techniques.

A series of batch tests were performed to determine the effects of independent variables (initial Ni concentration, solution pH, adsorbents' dosage, contact time) on Ni removal from aqueous solutions. To this end, a 25-mL solution containing different contents of Ni (30, 60, and 90 mg L^{-1} prepared from $Ni(NO_3)_2 \cdot 6H_2O$) with the desired pH (3, 5, and 7; set by 0.1 M NaOH and 0.1 M HCl solutions) was poured into sterile centrifuge tubes, and the prepared adsorbents (RBO and BC) at different doses (2.5, 5, and 7.5 g L^{-1}) were added to each tube separately. The tubes were shaken vigorously for 20, 40, and 60 min at 25°C±2 and then centrifuged at 3500 rpm. The supernatant was filtered, and the Ni concentration in the clear extract solution was determined using an atomic absorption spectrophotometer (Varian SpectrAA-10). The percentage of Ni removal (***q***) was calculated as:

$$q = \frac{C_i - C_f}{C_i} \times 100$$

where $\boldsymbol{C}_i$ and $\boldsymbol{C}_f$ are initial and final Ni concentrations (mg L^{-1}), respectively.

To investigate the effects of different factors and their interactions on Ni removal, and to optimize and predict the removal rate, the BBM under RSM was adopted to evaluate independent variables on response performance (Ni removal). The independent variables were the initial Ni^{+2} concentration (A), pH (B), adsorbent dose (C), and contact time (D) at three levels of minimum, medium, and maximum. The number of experiments required by BBM was determined from the equation N=2K(K-1)+C, where N is the number of test samples, K is the number of variables (n=4), and C is the number of central points (n=5). All the experiments based on BBD included 29 tests for each adsorbent. In the RSM, a model is defined for each dependent variable (Ni removal efficiency) that expresses the main and interaction effects of the factors on each independent variable. The RSM model employed to predict the optimal point is expressed as follows:

$$Y = \beta_0 + \sum_{i=1}^{m} \beta_i X_i + \sum_{i=1}^{m} \beta_{ii} X_i^2 + \sum_{j=i+1}^{m} \beta_{ij} X_i X_j + \varepsilon$$

where Y represents the predicted value of the response variables, β_0 is the intercept coefficient, β_i is the linear coefficient, β_{ii} is the quadratic coefficient, β_{ij} is the interaction coefficient, and ε is the residual term. The regression equations and response surface plots of RSM, to identify the optimum conditions of Ni removal, were generated by Design-Expert 7.00.

RESULTS AND DISCUSSION

The FTIR spectral analysis of RBO and BC samples (Fig. 1) shows that the pyrolysis process has increased the wavelengths of 566, 610, 1035, 1620, and 1450 cm^{-1}, which are responsible for the structure of well-crystallized apatite (vibrations of stretching and bending of phosphate) (Younesi et al., 2011; Figueiredo et al., 2010; Xu et al., 2008).

On the other hand, the pyrolysis process led to the disappearance of the functional groups with a vibrational structure at wavelengths of 2860-2930 cm^{-1} (C-H stretching functional groups), 1743 cm^{-1} (C = O stretching functional groups), 1556 (C = C stretching functional groups), and 812 cm^{-1} (CO_3^{2-} group) (Figueiredo et al., 2010). The spectral changes of the carbonate group

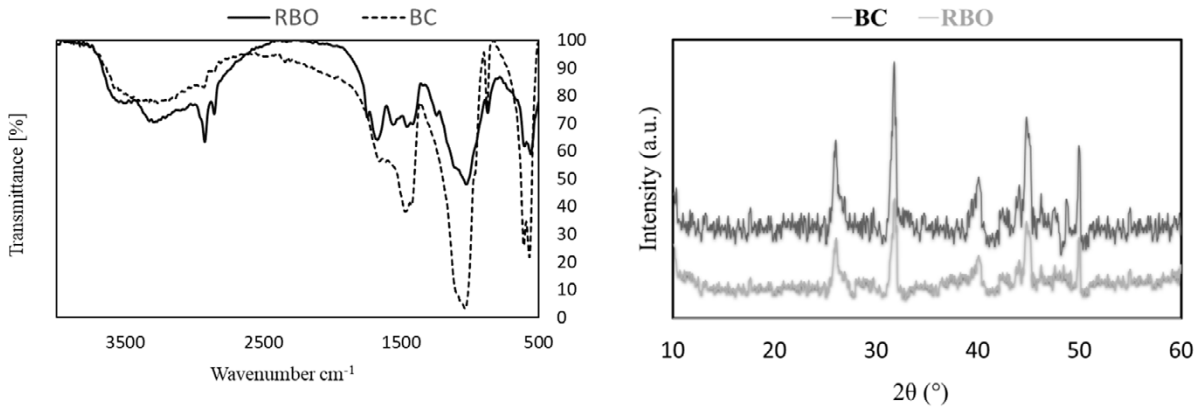

Fig 1. FTIR spectra (left) and XRD patterns (right) of RBO and BC.

Table 1. Selected physical and chemical properties of RBO and BC

Chemical composition						
Adsorbent	Elemental analysis				EDX results	
	C(%)	H(%)	N(%)	S(%)	Ca	Mg
RBO	15.27	2.70	4.36	0.21	26.96	2.15
BC	9.72	0.83	2.33	0.1	59.36	3.82
Porosity characteristics						
Adsorbent	BET surface area (m^2 g^{-1})		Total pore volume (cm^3 g^{-1})		Average pore diameter (nm)	
RBO	0.96367		0.0015642		6.4926	
BC	95.907		0.2365		9.8632	

band (873 cm^{-1}) indicated the same structure in both samples and did not show specific changes (Xu et al., 2008). The FTIR absorption spectra obtained in the BC sample of the present study were consistent with the findings of other researchers (Jia et al., 2018; Shahid et al., 2019). In general, based on the FTIR spectroscopy, pyrolysis enriched the phosphate functional groups and reduced the carbonate functional groups in the BC sample compared to the RBO sample, which were also evident in elemental analysis values. Based on the elemental analysis results, the pyrolysis process reduced the carbon content of the BC sample (9.72%) compared to RBO (15.27%) (Table 1). An examination of the quantity of hydrogen, nitrogen, and sulfur following the pyrolysis process also indicated a decrease in these elements in the composition of BC compared to RBO (Table 1). Mendoza-Castillo et al. reported the levels of carbon, hydrogen, nitrogen, and sulfur in BC as 11.65, 1.03, 1.21, and 0.06%, respectively (Mendoza–Castillo et al., 2015).

The XRD patterns of the RBO and BC are displayed in Fig 1. As it can be seen, the XRD pattern of both adsorbents contain diffraction peaks (2θ) at 25.9°, 31.7°, 40°, 45°, 46.8° and 49.8°, which correspond to the Ca5(PO4)3(OH) (calcium hydroxyapatite) structure. The intensity of these peaks in BC was obviously stronger than RBO, which indicating a better degree of crystallinity.

Figure 2 depicts the morphology of RBO and BC samples at different scales. Based on the results, the pyrolysis process results in the disappearance of the relatively regular RBO surface morphology, leading to a dense structure in BC. To put it simply, BC had smaller geometry components, irregular structure, and rougher surface area (per unit area) than RBO. In the morphology study of one kind of BC, Mesquita et al. (2017) reported that it has high porosity

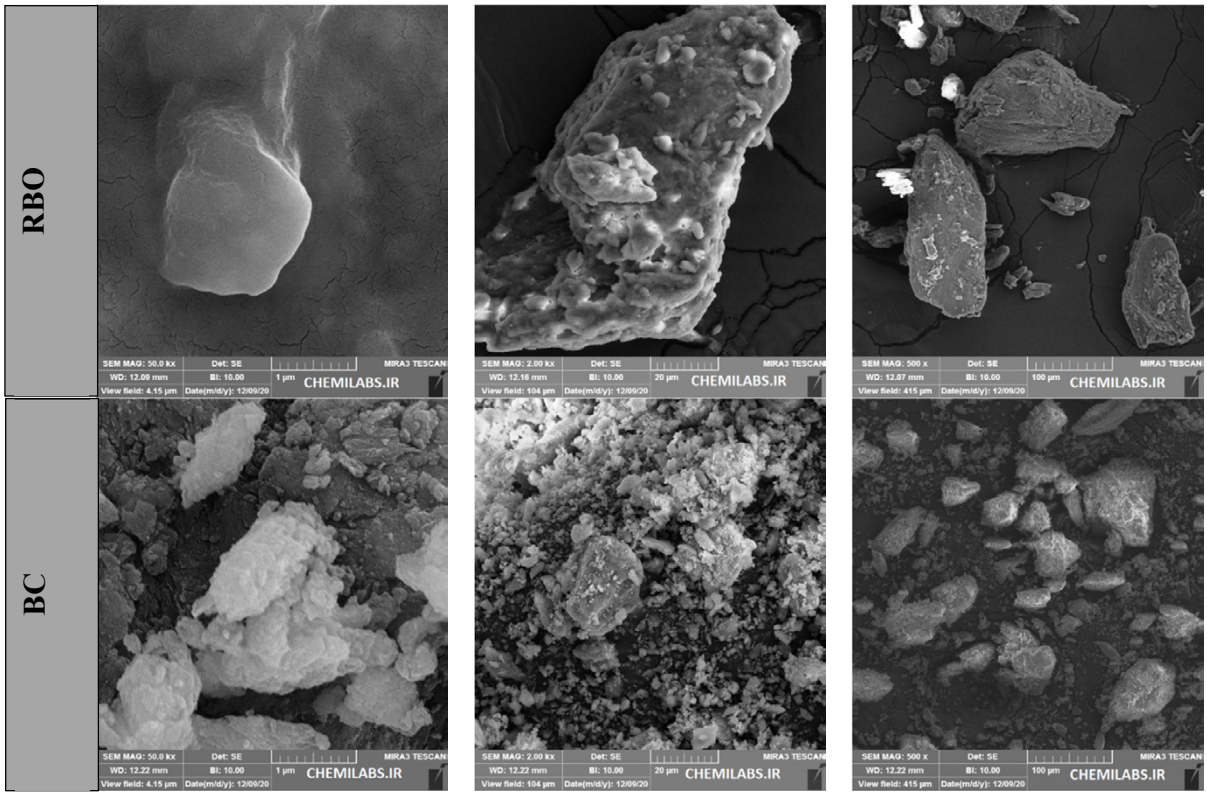

Fig 2. FE-SEM images of RBO and BC at different scales (1 μm, 20 μm , 100 μm).

and irregular structure on its surface. The evaluation of quantitative amounts of inorganic fractions obtained from the EDX analysis (Table 1) in present adsorbents revealed that the two main cations of calcium (Ca) and magnesium (Mg) that greatly contribute to ion exchange with metals (Pan et al., 2009) are higher in BC than RBO.

BET analysis of adsorbents showed that the values of specific surface area, total porosity volume, and average porosity diameter in RBO were 0.96 m2 g^{-1}, 0.001 cm3 g^{-1}, and 6.49 nm, respectively, while these values in BC were equal to 95.9 m2 g^{-1}, 0.236 cm3 g^{-1}, and 9.863 nm, respectively (Table 1). In the study of bovine BC structure (at 350 °C for 2 hours), Shahid et al. (2019) reported the values of specific surface area, total porosity volume, and average porosity diameter of 79.34 m2 g^{-1}, 0.041 cm3 g^{-1}, and 2.09 nm, respectively. Maeda et al. (2019) considered a bone char and showed that the specific surface area and average pore diameter were 109 m^2 g^{-1} and 94 Å, respectively. The evaluation of N_2 adsorption and desorption isotherms revealed that both adsorbents follow a type-IV isotherm based on the BDDT (Brunauer-Deming-Deming-Teller) classification (Figure 3).

The pattern of type-IV isotherm indicates the structure of mesopores in two adsorbents. In other words, the type-IV isotherm has a hysteresis loop associated with the presence of mesopores in the adsorbent, which is a sign of capillary density in these pores; therefore, the adsorption process is limited in a high relative pressure range (p_0/p). Moreover, according to the IUPAC classification, a hysteresis loop of type H3 was observed in RBO and BC. A hysteresis loop indicates the presence of mesopores in the adsorbents' structure. Similar results have been reported by Coltre et al. (2020). Isotherms following type H3 typically cover a wide range from meso to micro and larger pores. However, the isotherms following type H3 often have meso/micro pores, which are assembled by the loose stacking of flaky particles and a matrix of fine pores, and resulting in their geometric shape as a wedge-shaped pore (Xu et al., 2020).

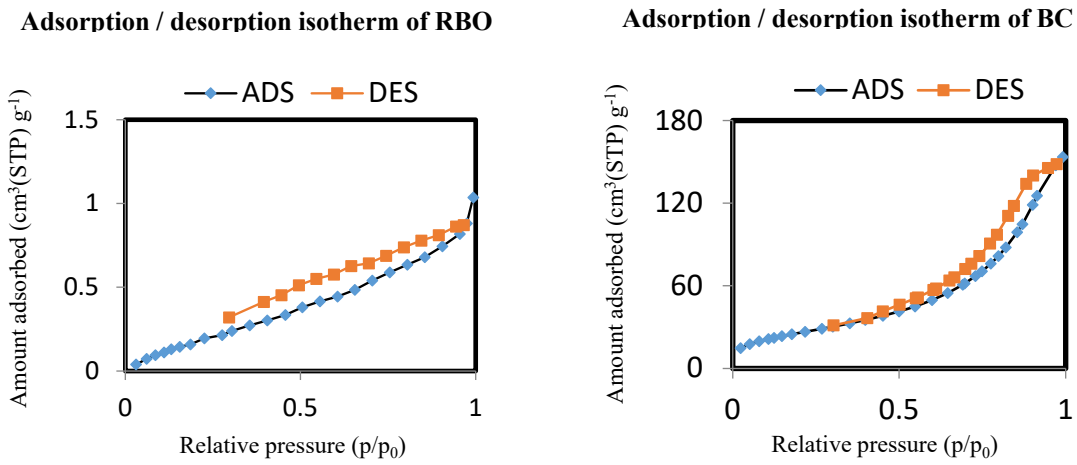

Fig 3. N_2 adsorption–desorption isotherms of RBO and BC

Table 2. Experimental design based on BBM used in this study

Test No	(A)	(B)	(C)	(D)	R(%) **RBO**	R(%) **BC**	Test No	(A)	(B)	(C)	(D)	R(%) **RBO**	R(%) **BC**
1	90	3	5	40	6.10	32.67	16	60	7	2.5	40	28.00	53.00
2	60	5	2.5	60	23.00	48.17	17	60	3	2.5	40	3.50	36.50
3	30	5	5	60	28.00	70.67	18	90	5	7.5	40	20.67	46.44
4	60	5	7.5	60	27.67	54.67	19	60	7	7.5	40	34.00	59.67
5	90	5	2.5	40	13.89	40.78	20	90	7	5	40	17.11	44.44
6	60	3	5	20	9.17	38.00	21	30	5	2.5	40	19.67	62.33
7	60	3	5	60	16.00	41.17	22	60	5	2.5	20	18.67	43.00
8	60	3	7.5	40	14.17	44.50	23	60	7	5	20	22.90	51.33
9	60	5	5	40	24.75	51.33	24	30	5	5	20	28.00	68.33
10	60	5	5	40	26.67	52.17	25	60	5	5	40	24.33	51.00
11	60	7	5	60	37.33	62.83	26	30	5	7.5	40	38.00	74.67
12	90	5	5	20	2.89	37.67	27	90	5	5	60	12.44	40.00
13	60	5	5	40	20.67	50.83	28	30	7	5	40	43.00	79.33
14	60	5	7.5	20	31.83	56.33	29	30	3	5	40	19.67	59.00
15	60	5	5	40	27.00	52.00							

(A): Initial concentration of Ni (ppm); **(B)**: pH solution; **(C)**: Adsorbent dose (g l^{-1}); **(D)**: Time contact (min); R(%) **RBO**: Ni removal (%) by RBO; **BC**: Ni removal (%) by **BC**

According to the reports of Xu et al., the type H3 hysteresis loop indicates the existence of only an external special surface (no internal special surface) (Xu et al., 2020); according to the type of porosity (mesopore or micropore) existing in the edges of the studied adsorbent, and the very high adsorption of N_2 in the BC sample compared to RBO (Figure 3), it seems that the porosity created in BC is microporous and that created in RBO is mesoporous or macroporous.

Table 2 lists the Ni removal values in the presence of RBO and BC, under the control of various factors. As a result, Ni's affinity for the studied adsorbents markedly differed. In view of the results, BC removed Ni more effectively than RBO. The Ni removal percentage in BC and RBO was 32.67-79.3% (average 51.8%) and 2.89-43% (average 22%), respectively. The

inorganic structure of BC plays an important role in the adsorption of metal ions. According to previous reports, the inorganic part of BC has an acceptable ion exchangeability between metal cations and Ca^{2+}. In the studies by Corami et al. (2008) and Mendoza-Castillo et al. (2015), when evaluating the rate of Ca^{2+} release before and after the adsorption process of some elemental cations by BC, it was found that ion exchangeable was the main mechanism in heavy metal absorption. However, when assessing heavy metal adsorption by acid-modified BCs, due to the low rate of Ca^{2+} release, surface complex formation was expressed as the main mechanism of element adsorption (Mendoza–Castillo et al., 2015). Higher values of Ca^{2+} and Mg^{2+} in the present BC compared to RBO (Table 1) indicate the presence of more ion-exchangeable sites and, thus, higher Ni^{2+} adsorption values. An element is substituted with Ca^{2+} when it has an ionic radius smaller than the ionic radius of Ca (1.74 A°). Due to the low ionic radius of Ni^{+2} (1.21 A°) compared to Ca^{2+}, Ni^{+2} can easily replace Ca^{2+} ions in BC. It is also hypothesized that the pyrolysis process, which causes Ca^{2+} ion enrichment in BC, results in a higher exchange rate of Ca^{2+} than RBO, which in turn increases the Ni^{2+} exchangeable mechanism. According to the following equation, Ca^{2+} is exchanged with Ni^{2+} (■ shows the surface of BC).

$$■Ca^{2+}(s) + Ni^{2+}(aq) = ■\ Ni^{2+}(s) + \ Ca^{2+}(aq)$$

Furthermore, due to the existence of a hydroxyapatite structure in BC, the following reaction is also possible and occurs:

$$■OH + Ni^{2+} = ■\ O - Ni^{+} + \ H^{+}$$

In addition, due to the higher specific surface area of BC (100 times) compared to RBO, the physical adsorption of Ni^{2+} along with the ion exchangeable mechanism has increased the adsorption of Ni^{2+} by 2.3 times.

Based on the results of fitting the model of BBM on Ni^{2+} removal data by two adsorbents, the reduced cubic model had the best fit among the independent factors and Ni^{2+} removal (Table 3).

The F-values of 19.38 and 362, as well as P-values <0.0001 for both adsorbents indicate that the selected models have a proper fit and are statistically significant for simulating Ni^{2+} removal from aqueous solutions. The close values of R^2 and adjusted R^2 in the models fitted to both adsorbents indicate an acceptable correlation between the observed and predicted values. An adequate precision value (indicating the signal-to-noise ratio) >4 demonstrates appropriate modeling in predicting Ni^{2+} removal by two adsorbents. Moreover, the obtained probability of lack of fit (LOF) >0.05 shows that the BBM used in the current study is statistically significant for prediction, and is suitable for further analysis.

Given the proper fit of the reduced cubic model on Ni^{2+} removal variables by two adsorbents, the following equations (1 and 2) were obtained:

(Eq. 1) Removal of Ni by RBO=+22.83-8.60A+9.48B+4.97C+1.22D+1.90BD-1.92B^2+4.10B^2D

(Eq. 2) Removal of Ni by BC=+51.47-15.32A+8.23B+4.73C+1.02D-2.14AB-1.67AC-0.33BC+2.08BD-1.71CD+4.41A^2-2.32B^2-0.12C^2-1.11D^2+2.87AC^2-1.06B^2C+2.65B^2D

where A, B, C, and D denote the Ni^{2+} concentration, pH, adsorbent dosage, and contact time, respectively.

According to Eq. 2, the three-dimensional (3D) diagrams of independent variables' effects on Ni^{2+} removal by BC were plotted (Figure 4). The evaluation of pH and Ni^{2+} initial concentration interactions showed that, at low concentrations of Ni^{2+}, by raising the pH, Ni^{2+} removal significantly increased; nevertheless, at high concentrations, the magnitude of this increase was smaller. In addition, in different pH ranges, by raising the Ni^{2+} concentration, Ni^{2+} removal significantly decreased.

Table 3. Analysis of variance (ANOVA) of the BBM for Ni removal

	Sum of squares	Degree of freedom	Mean square	F-value	Probability > F
Adsorbent of RBO					
Model	2427.613	7	346.8018	19.38143	< 0.0001
Residual	375.7638	21	17.89351		
Lack of fit	350.2027	17	20.60016	3.223672	0.1328
Pure error	25.56111	4	6.390278		
Total	2803.377	28			
R^2 = 0.868; Adjusted R^2=0.821; Predicted R^2=0.761; CV=19.20%; Adequate precision:16.2					
Adsorbent of BC					
Model	3871.919	16	241.995	362.0334	< 0.0001
Residual	8.021193	12	0.668433		
Lack of fit	6.610082	8	0.82626	2.342155	0.2143
Pure error	1.411111	4	0.352778		
Total	3879.941	28			
R^2 = 0.997; Adjusted R^2=0.995; Predicted R^2=0.978; CV=1.58%; Adequate precision:75.24					

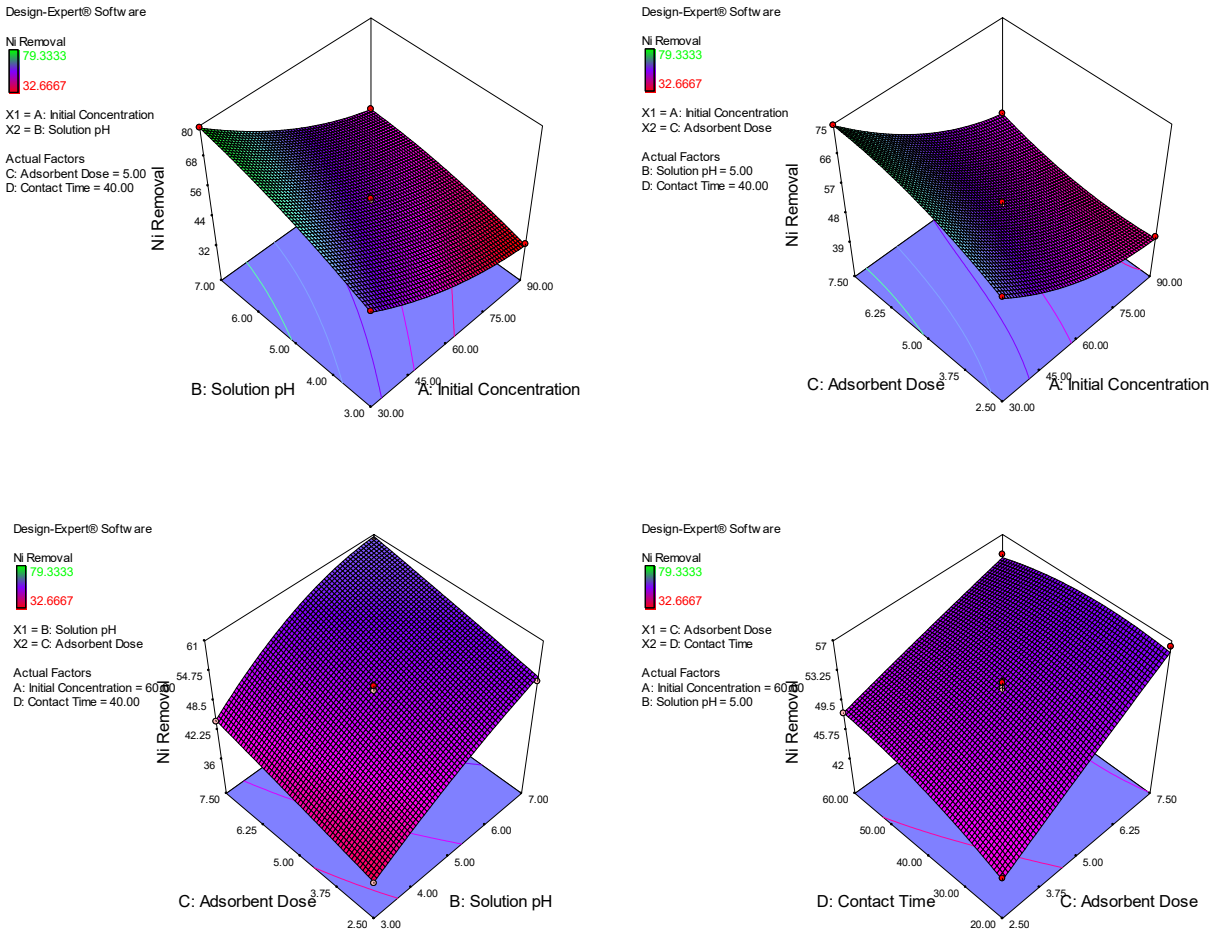

Fig 4. Interaction effects of independent variables on Ni removal efficiency under predefined conditions, affected by BC application.

The results of the interactions between the adsorbent dose and the initial concentration of Ni^{2+} revealed that, at different concentrations of initial Ni^{2+}, by raising the adsorbent dose, the removal of Ni^{2+} increased; however, this increase was more noticeable at lower levels of Ni^{2+} initial concentration.

The investigation of adsorbent dose and pH interactions on Ni^{2+} removal showed that, in different pH ranges, with increasing the adsorbent dose, the removal of Ni^{2+} was enhanced. Moreover, in different ranges of adsorbent dose, with raising the pH, Ni^{2+} removal demonstrating a rising trend; still, this increase was more evident at a lower absorbent dose.

The interaction effect of initial Cd concentration and adsorbent dose revealed that, at different contact times and at low adsorbent doses, the Ni^{2+} removal was incremental, which was less evident at a low level of contact time. In contrast, at low levels of adsorption, the Ni^{2+} removal rate increased with raising the contact time, whereas at high levels of adsorbent, the Ni^{2+} removal trend was relatively decreasing with increasing the contact time.

According to the findings, by reducing the solution pH in the presence of the studied adsorbents, the removal of Ni^{2+} decreased, which can be explained by the presence of more H^+ ions which increased the repulsion between Ni^{2+} and H^+ and ultimately reduced Ni^{2+} adsorption. In other words, at higher pH, with increasing the OH^- ions, the adsorption surfaces became more negative and, thereby, the electrostatic adsorption between Ni^{2+} and the adsorbent surfaces increased (Saffari et al., 2018).

Furthermore, since the values of pH_{ZPC} (zero point of charge) of the adsorbent RBO and BC were 5.2 and 5.8, respectively (data are not shown), at a pH higher than these values, the adsorbent surfaces had higher values of negative charge and, therefore, the Ni^{2+} removal increased. In summary, at a pH lower than pH_{ZPC}, the adsorbent surface is positive and the adsorption is of the exchangeable type, while at values higher than $pH_{ZP}C$, the adsorption process is electrostatic. By increasing pH, the Ni^{2+} adsorption rose, indicating that the adsorption of Ni^{2+} is electrostatic. Various studies have reported that heavy metal adsorption is increased by raising pH (Ghomri et al., 2013; Božić et al., 2013). As the Ni^{2+} concentration increases, the adsorption sites on the adsorbent surfaces decrease (due to the saturation of the adsorption sites) and, thus, the adsorption decreases. In various studies, increasing the initial concentration of heavy metals reduces the adsorption efficiency (Saffari et al., 2018). Moreover, as the adsorbent dose rises, the active adsorption sites available for Ni^{2+} are increased, thereby promoting Ni^{2+} removal.

Herein, optimization of Ni^{+2} removal and model desirability were obtained using the numerical optimization method. To obtain the maximum efficacy, according to the objectives of the research, the independent factors were considered within their normal range, and the response (Ni removal) at the maximum value. Based on the findings, 30 solutions were obtained, and the first 10 solutions for the studied adsorbents are given in Table 4.

Table 4. Experimental results for model validation conducted at the optimum conditions as obtained from BBM in each adsorbent.

Adsorbent of RBO							Adsorbent of BC						
Solution	**(A)**	**(B)**	**(C)**	**(D)**	R(%)	**DE**	Solution	**(A)**	**(B)**	**(C)**	**(D)**	R(%)	**DE**
1	30.11	6.97	4.04	59.22	43.7851	1	1	30.79	6.99	4.87	57.82	82.5631	1
2	30.41	6.77	6.46	50.4	44.2803	1	2	30.17	6.48	7.17	55.65	81.3327	1
3	40.61	6.92	5.67	59.7	43.8092	1	3	30.15	6.86	6.64	55.56	83.3629	1
4	31.25	6.92	5.89	51.52	44.0734	1	4	30.2	6.29	5.84	49.74	79.477	1
5	34.11	6.99	6.91	46.84	44.0309	1	5	30.01	6.07	6.86	59.95	79.3338	1
6	32.57	6.91	6.97	49.4	45.1088	1	6	30.03	6.65	7.49	33.82	79.5755	1
7	51.95	6.95	7.27	58.33	43.4832	1	7	31.28	6.38	6.26	53.39	79.6774	1
8	33.5	6.85	6.86	49.85	44.4306	1	8	31.59	6.97	6.97	37.93	79.4651	1
9	30.03	6.71	6.28	56.18	45.3608	1	9	30.08	6.88	5.12	42.57	79.7311	1
10	31.52	6.87	6.29	53.92	45.3421	1	10	30.63	6.42	7.41	39.58	79.4648	1

(A): Initial concentration of Ni (ppm); **(B)**: pH solution; **(C)**: Adsorbent dose (g l^{-1}); **(D)**: Time contact (min); R(%): Ni removal; **DE**: Desirability

The maximum removal of Ni^{+2} (43.7%) in adsorbent RBO was found at an Ni^{+2} initial concentration of 30 mg L^{-1}, pH of 6.97, adsorbent dose of 4.04 g L^{-1}, and contact time of 59.22 min, with the desirability of 1. On the other hand, the maximum value of Ni^{+2} removal (82.56) with BC was achieved at the initial Ni^{+2} concentration of 30.79 mg L^{-1}, pH of 6.99, adsorbent dose of 4.87 g L^{-1}, and contact time of 57.82 min, with the desirability of 1 (Table 4). Hosseini et al. (2016) studied the optimization of Ni removal from an aqueous solution by natural zeolite using RSM. Based on their numerical optimization results, the optimum removal was obtained at an initial Ni ion concentration of 10–15 mg L^{-1}, clinoptilolite dosage of 0.37–0.43 g L^{-1}, a contact time of 56–68 min, and a pH of 4.8–6. In investigating the effects of various factors on the removal of Ni by agricultural waste biomass using RSM, the optimum conditions for maximum Ni removal from an aqueous solution of 50 mg L^{-1} were found to be adsorbent dose (1500 mg L^{-1}), pH (7.52), and stirring speed (150 rpm) (2008).

CONCLUSIONS

Herein, the efficiency of Ni removal by raw bone and its biochar, influenced by various adsorption factors, was investigated. The calcination process slightly increased the phosphate functional groups and the specific surface area in BC. The existence of higher contents of Ca as an exchangeable metal cation, and a higher specific surface area and porosity in BC compared to RBO, caused the removal of more Ni in aqueous solutions. The investigation of effective factors on Ni removal demonstrated the direct effects of pH and adsorbent dose, as well as inverse effects with initial Ni concentration. The prediction made by the RSM had high validity, and the BBM could well predict Ni removal. The maximum adsorption obtained from BC (as the superior adsorbent) was achieved at an initial Ni^{2+} concentration of 30.79 mg L^{-1}, pH of 6.99, adsorbent dose of 4.87 g L^{-1}, and contact time of 57.82 min, with the desirability of 1. BC is expected to show greater Ni removal ability, but the application of modification processes in BC (including physical and chemical activation) may help improve the removal efficiency of heavy metals.

ACKNOWLEDGMENTS

The authors would like to acknowledge the financial support of the Institute of Science and High Technology and Environmental Sciences, Graduate University of Advanced Technology (Kemran-Iran).

GRANT SUPPORT DETAILS

This research has been supported by the Institute of Science and High Technology and Environmental Sciences, Graduate University of Advanced Technology (Kemran-Iran).

CONFLICT OF INTEREST

The authors declare that there is not any conflict of interests regarding the publication of this manuscript. In addition, the ethical issues, including plagiarism, informed consent, misconduct, data fabrication and/ or falsification, double publication and/or submission, and redundancy has been completely observed by the authors.

LIFE SCIENCE REPORTING

No life science threat was practiced in this research.

REFERENCES

Alkurdi, S. S., Al-Juboori, R. A., Bundschuh, J. and Hamawand, I. (2019). Bone char as a green sorbent for removing health threatening fluoride from drinking water. Environ. Int., 127; 704-719.

Alkurdi, S. S., Al-Juboori, R. A., Bundschuh, J., Bowtell, L. and McKnight, S. (2020). Effect of pyrolysis conditions on bone char characterization and its ability for arsenic and fluoride removal. Environ. Pollut., 262; 114221.

Božić, D., Gorgievski, M., Stanković, V., Štrbac, N., Šerbula, S. and Petrović, N. (2013). Adsorption of heavy metal ions by beech sawdust–Kinetics, mechanism and equilibrium of the process. Ecol. Eng., 58; 202-206.

Corami, A., Mignardi, S. and Ferrini, V. (2008). Cadmium removal from single-and multi-metal (Cd+ Pb+ Zn+ Cu) solutions by sorption on hydroxyapatite. J. Colloid Interface Sci., 317(2); 402-408.

Mesquita, P. D. L., Cruz, M. A. P., Souza, C. R., Santos, N. T. G., Nucci, E. R. and Rocha, S. D. F. (2017). Removal of refractory organics from saline concentrate produced by electrodialysis in petroleum industry using bone char. Adsorption, 23(7); 983-997.

Coltre, D. S. D. C., Cionek, C. A., Meneguin, J. G., Maeda, C. H., Braga, M. U. C., de Araújo, A. C. and Arroyo, P. A. (2020). Study of dye desorption mechanism of bone char utilizing different regenerating agents. SN Appl. Sci., 2(12); 1-14.

Figueiredo, M. J. D. F. M. D., Fernando, A., Martins, G., Freitas, J., Judas, F. and Figueiredo, H. (2010). Effect of the calcination temperature on the composition and microstructure of hydroxyapatite derived from human and animal bone. Ceram. Int., 36(8); 2383-2393.

Garg, U. K., Kaur, M. P., Garg, V. K. and Sud, D. (2008). Removal of nickel (II) from aqueous solution by adsorption on agricultural waste biomass using a response surface methodological approach. Bioresour. Technol., 99(5); 1325-1331.

Genchi, G., Sinicropi, M. S., Lauria, G., Carocci, A. and Catalano, A. (2020). The effects of cadmium toxicity. Int. J. Environ. Res. Public, 17(11); 3782.

Ghanizadeh, G. and Asgari, G. (2011). Adsorption kinetics and isotherm of methylene blue and its removal from aqueous solution using bone charcoal. React. Kinet. Mech. Catal., 102(1); 127-142.

Ghomri, F., Lahsini, A., Laajeb, A. and Addaou, A. (2013). The removal of heavy metal ions (copper, zinc, nickel and cobalt) by natural bentonite. Larhyss J., 12; 37-54.

Hassan, S. S., Awwad, N. S. and Aboterika, A. H. (2008). Removal of mercury (II) from wastewater using camel bone charcoal. J. Hazard. Mater., 154(1-3); 992-997.

Hosseini, S. S. S., Khosravi, A., Tavakoli, H., Esmhosseini, M. and Khezri, S. (2016). Natural zeolite for nickel ions removal from aqueous solutions: Optimization and modeling using response surface methodology based on central composite design. Desalin. Water Treat., 57(36); 16898-16906.

Ida, S. and Eva, T. (2021). Removal of heavy metals during primary treatment of municipal wastewater and possibilities of enhanced removal: A review. Water, 13(8); 1121.

Jia, P., Tan, H., Liu, K. and Gao, W. (2018). Synthesis, characterization and photocatalytic property of novel ZnO/bone char composite. Mater. Res. Bull., 102; 45-50.

Maeda, C. H., Araki, C. A., Moretti, A. L., de Barros, M. A. S. D. and Arroyo, P. A. (2019). Adsorption and desorption cycles of reactive blue BF-5G dye in a bone char fixed-bed column. Environ. Sci. Pollut. Res., 26(28); 28500-28509.

Mendoza-Castillo, D. I., Bonilla-Petriciolet, A. and Jáuregui-Rincón, J. (2015). On the importance of surface chemistry and composition of bone char for the sorption of heavy metals from aqueous solution. Desalin. Water Treat., 54(6); 1651-1662.

Pan, X., Wang, J. and Zhang, D. (2009). Sorption of cobalt to bone char: Kinetics, competitive sorption and mechanism. Desalin., 249(2); 609-614.

Saffari, M. (2018). Response surface methodological approach for optimizing the removal of cadmium from aqueous solutions using pistachio residues biochar supported/non-supported by nanoscalezero-valent iron. Main Group Met. Chem., 41(5-6); 167-181.

Shahid, M. K., Kim, J. Y. and Choi, Y. G. (2019). Synthesis of bone char from cattle bones and its application for fluoride removal from the contaminated water. Groundw. Sustain. Dev., 8; 324-331.

Shahid, M. K., Kim, J. Y., Shin, G. and Choi, Y. (2020). Effect of pyrolysis conditions on characteristics and fluoride adsorptive performance of bone char derived from bone residue. J. Water Process. Eng., 37; 101499.

Wang, M., Liu, Y., Yao, Y., Han, L. and Liu, X. (2020). Comparative evaluation of bone chars derived from

bovine parts: Physicochemical properties and copper sorption behavior. Sci. Total Environ., 700; 134470.
Xu, H., Yang, L., Wang, P., Liu, Y. and Peng, M. (2008). Kinetic research on the sorption of aqueous lead by synthetic carbonate hydroxyapatite. J. Environ. Manage., 86(1); 319-328.
Xu, L., Zhang, J., Ding, J., Liu, T., Shi, G., Li, X., ... and Guo, R. (2020). Pore structure and fractal characteristics of different shale lithofacies in the dalong formation in the western area of the lower yangtze platform. Minerals, 10(1); 72.
Younesi, M., Javadpour, S. and Bahrololoom, M. E. (2011). Effect of heat treatment temperature on chemical compositions of extracted hydroxyapatite from bovine bone ash. J. Mater. Eng. Perform, 20(8); 1484-1490.